

Indirect torque observer-based sensor-less efficient control of bearingless switched reluctance motor using global sliding mode and square currents control method

Pulivarthi Nageswara RAO, Ramesh DEVARAPALLI, Fausto Pedro García MÁRQUEZ,
G. V. Nagesh KUMAR and Behnam MOHAMMADI-IVATLOO

The Bearingless Switched Reluctance Motor (BSRM) is a new technology motor, which overcomes the problems of maintenances required associated with mechanical contacts and lubrication of rotor shaft effectively. In addition, it also improves the output power developed and rated speed. Hence, the BSRM can achieve high output power and super high speed with less size and cost. It has a considerable ripple in the net-torque due to its critical non-linearity and the salient pole structures of both stator and rotor poles. The resultant torque ripple, especially in these motors, causes the more vibrations and acoustic noises will affects the levitated rotor safety also. Practically at high-speed operations, the accurate measurement of the rotor position is complicated for conventional mechanical sensors. A new square currents control with global sliding mode control based sensorless torque observer is proposed to minimize the torque ripple and achieve a smooth, robust operation without using any mechanical sensors. The proposed controller is designed based on the error between the reference and measured torque values. The sliding mode torque observer measures the torque from the actual phase voltages, currents, and look-up tables. The simulation model has been modelled to validate the proposed methodology. From the simulation outputs, it is clear that the reduction of torque ripple by the proposed

Copyright © 2021. The Author(s). This is an open-access article distributed under the terms of the Creative Commons Attribution-NonCommercial-NoDerivatives License (CC BY-NC-ND 4.0 <https://creativecommons.org/licenses/by-nc-nd/4.0/>), which permits use, distribution, and reproduction in any medium, provided that the article is properly cited, the use is non-commercial, and no modifications or adaptations are made

P.N. Rao (e-mail: nnageshmtech@gmail.com) is with Department of Electrical Electronics and Communication Engineering, Gandhi Institute of Technology and Management (Deemed to be University), Visakhapatnam, 530045, Andhra Pradesh, India.

R. Devarapalli (e-mail: ramesh.ee@bitsindri.ac.in) is with Department of Electrical Engineering, BIT Sindri, Dhanbad 828123, Jharkhand, India.

F.P. García Márquez (corresponding author, e-mail: FaustoPedro.Garcia@uclm.es) is with Ingenium Research Group, University of Castilla-La Mancha, Spain.

G.V. Nagesh Kumar (e-mail: drgvnk14@gmail.com) is with Department of EEE, JNTU Anantapur, College of Engineering, Pulivendula-516390, Andhra Pradesh, India.

B. Mohammadi-Ivatloo (e-mail: mohammadi@ieee.org) is with University of Tabriz, Tabriz, Iran.

The work reported herewith has been financially by the Dirección General de Universidades, Investigación e Innovación of Castilla-La Mancha, under Research Grant ProSeaWind project (Ref.: SB-PLY/19/180501/000102).

Received 9.10.2020. Revised 18.01.2021.

method shows improved than the conventional sliding mode controller. The overall system is more robust to the external disturbances, and it also gets efficient torque profile.

Key words: bearingless, global sliding mode, efficient: maintenance, safety, torque ripple

1. Introduction

The switched reluctance motor (SRM) is not used in all industrial applications for a long time because of its acoustic noise, which is produced from broad ripples, in net torque [1, 2]. However, in recent years, with the support of robust control technics and modern power electronic devices, the SRM has been initiated to be used in electric vehicle and many industrial applications [3–6]. The bearing-less concept is an alternative to the magnetic bearing drives because of its advantages [7], such as less price, compact in size and not at all necessity of high-performance power amplifiers. The bearingless switched reluctance motor (BSRM) shows considerable ripples in the torque because of its critical non-linearity and the salient pole structures of both stator and rotor poles, which makes smooth uneven operation at low and high-speed regions [8–10]. Although owing to the stepping operation of the motor, an unwanted vibration effect produces on the levitation of the rotor and makes an acoustic noise [11–13]. In addition to the mentioned advantages, the BSRM has the difficulties of accurate realization and accurate controlling due to its suspended rotor and its nonlinear magnetization characteristics [14, 15].

Therefore, the various suitable methods of torque ripple reduction techniques are required to overcome the mentioned drawbacks. The closed-loop torque control is unavoidable to get better torque profiles of BSRM. Closed-loop torque control has done in different methods of operations, namely single pulse control, voltage control and current control [16, 17]. The primary method has to minimize the resultant torque ripple by controlling the individual phase torques. Here, the reference torque values have distributed into each phase torques according to the rotor positions and torque sharing function (TSF) [18, 19]. However, the TSF based control techniques maybe lead to a loss of robustness of the whole system. Another condition of this method was that need of a huge memory for storage of torque sharing functions when many torque levels were desire in a wide speed range of control applications.

In general, a built-in rotor position sensor is needed to control the speed and torque of the BSRM, which increases the cost, size, and complexity of the BSRM drive. A simple linear or analytic controller cannot be reliable for BSRM, because of its nonlinear operational characteristics to reduce the cost and complexity of the BSRM, an observer-based robust controller is required [20]. The sliding mode torque observer (SMTO) has the benefits of fast response and robustness [21]. On the other hand, the SMTO has a problem with the operation of the asymmetric

converter, which is hanging onto the present state until the output state of the hysteresis controller's varied, i.e., the torque ripple produced is high [22,23]. The modelling-based control of the sum of the square current's method, along with SMTO, can solve the above problem. The torque ripple occurs mainly due to the addition of uncontrolled phase currents which are in increasing in the phase commutation period, but the resultant torque having nonlinear functions with the square of the phase currents [24–26].

In this paper, a regulated sum of squared currents is used to reduce the torque ripple along with the global sliding mode control (GSMC). The GSMC is designed based on the error between reference torque and measured torque values. The proposed control method has a fast-dynamic response and robust characteristics, regardless of the variation of the motor parameters. The stability of the proposed method has analyzed by Lyapunov function [27, 28]. The SMTO modelling is carried out using the support of real phase voltages, currents, flux linkages and torque look-up tables [29–31]. An error rectification term is realized subject to the difference between the actual regulated phase currents to the estimated phase current values [32–34].

The main contributions of this paper are:

- Design and modelling of global sliding mode torque controller-based sensorless SMTO to minimize the torque ripple along with square currents control method.
- A comparison study has taken between the robust controllers like conventional sliding mode control (SMC) and proposed GSMC based SMTO in the way of getting minimized torque ripple and robust torque profiles under different parameter variation conditions.
- The complete BSRM mathematical modelling was done by considering of non-linearities and magnetic saturation of both the windings.
- The finite element method is used to analyze characteristics of the recommended structure, which comprises magnetic flux distribution, inductance, torque and suspending force. In addition to its decoupled nature, the short flux paths in the stator and eccentric effects has also discussed.
- The converter based power electronic operation and its modes of operation, switching rules, also switching control strategy, converter topology has also discussed.
- The proposed methodology has been validated via simulation model. From the obtained results, it is clear that the torque ripple reduction by the proposed method has better than conventional SMC. The overall system exhibits more robust to the external disturbances.

The paper is structured as follows: In Section 2, operating principle and modeling of BSRM is discussed; In Section 3, the proposed square currents control method along with global sliding mode torque controller modellings are presented. The sensor-less SMTO design is described in this section. The dynamic simulation is carried out considering the above modellings; A complete, robust behaviour and minimized torque ripple properties have observed and discussed in Section 4; Section 5 concludes the work performed and the observations made during the progress.

2. Working principle and modeling of BSRM

2.1. Working principle

The poles of stator and rotor have salient type structures. Both torque winding and suspension windings have wound the stator separately. The intermittent and unidirectional excitation currents are given to each type of windings individually [35–37]. To get the continuous rotation of the rotor, the stator is excited sequentially with support of switching circuits [38, 39]. Therefore, the choosing of controllers for BSRM is additional difficult due to its nonlinear magnetic field circulation [40]. The basic 12/14 BSRM construction and its winding arrangement are shown in Fig. 1.

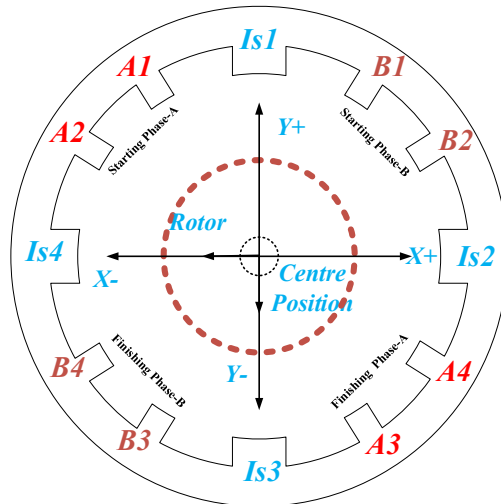


Figure 1: Configuration and winding arrangement of the stator

The regulated direct current (DC) voltages are applied to the stator torque coils and suspension coils individually to achieve the decoupled performance,

among net radial suspension force and resultant torques. The coordinately placed suspension winding coils I_{s1} , I_{s3} and I_{s2} , I_{s4} on the stator produces the radial forces in Y and X directions, respectively. In which, I_{s2} and I_{s1} produces the positive suspension forces, and I_{s4} and I_{s3} poles produce the negative suspension forces to make uniform and equilibrium stable levitation action. The remaining stator main phase coils named as phase-A and phase-B will produce the resultant rotational torque. The operating parameters and ratings of the 12/14 BSRM are given in Table 1.

Table 1: Operating details of 12/14 BSRM

Rated BSRM details	Value
Total input power to the motor	1000 W
Current/phase (maximum)	4 A
Applied per phase voltage	250 V
Net desired torque	1 Nm
Rated desired Speed	9000 rpm
Main winding per phase resistance	0.86 Ω
Levitation winding per phase resistance	0.32 Ω
Suspension voltage	250 V
Suspension current (maximum)	4 A

For maintaining the levitation force as continuous, the suspension force pole arc is chosen as more than one-rotor pole pitch according to references [25-27]. Hence, equal pole arcs dimension can be observed for both the suspension and rotor poles.

2.2. Finite element method analysis

The torque and currents have not directly linked in BSRM due to its fundamental operating principle [41, 42]. Hence the motor torque profile is always a nonlinear relation to the operating current and rotor position. The finite-element method based simulations offer the best accurate motor models. These numerical data and physical appearance characteristics can be used directly in any controller and observer designs. The flux distribution patterns of all excited suspension windings are shown in Fig. 2.

Similarly, the individual flux distribution patterns of main windings with short flux paths without flux reversal in the stator core are shown in Fig. 3a and b for phase A and B, respectively. The short flux paths in the stator core reduce core losses, and hence, there is a less requirement of magneto motive force (MMF).

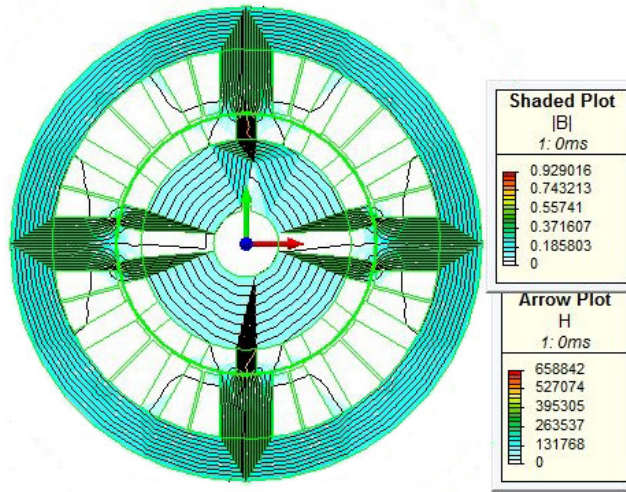


Figure 2: Uniform flux distribution of suspension windings

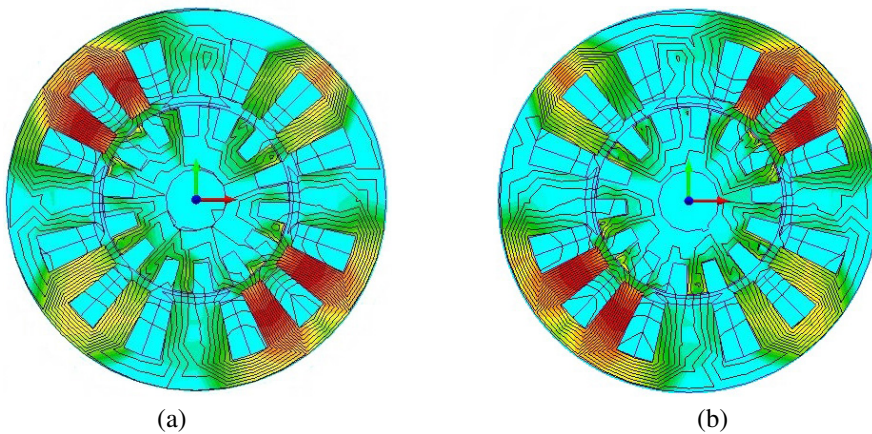


Figure 3: Short flux distributions of torque windings (a) Phase-A; and (b) Phase-B

The main torque winding and suspension winding inductance values are shown in Figs. 4 and 5 at different current values. The main torque winding inductance varies with rotor positions, see Fig. 4, reaching its maximum value when the rotor and stator poles get overlapped position.

Similarly, as it is shown in Fig. 5, the inductance profile of the suspension winding is almost constant, and it does not vary with rotor position due to the pole arc of the suspension pole is same as rotor pole arc.

The nonlinear torque profile of the main windings at different phase current values are shown in Fig. 6. Figure 6 shows that the main torque is a function of

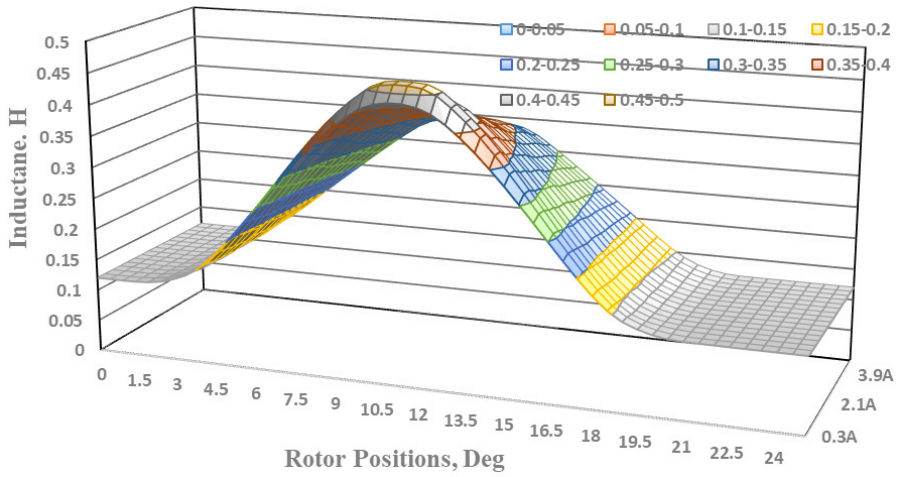


Figure 4: Inductance profile of main winding at different phase currents

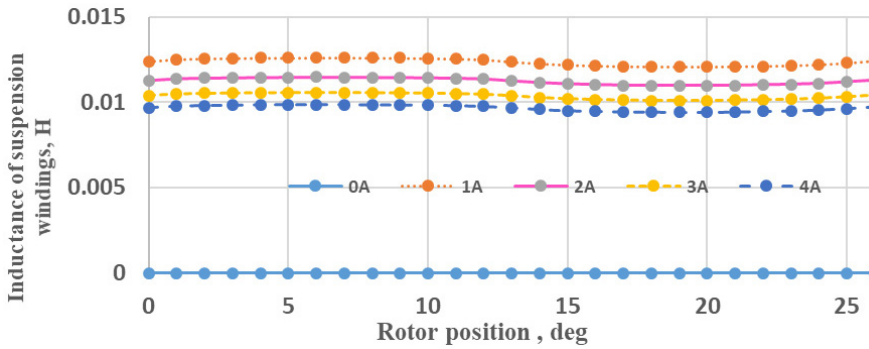


Figure 5: Inductance values of suspension winding at different suspension currents

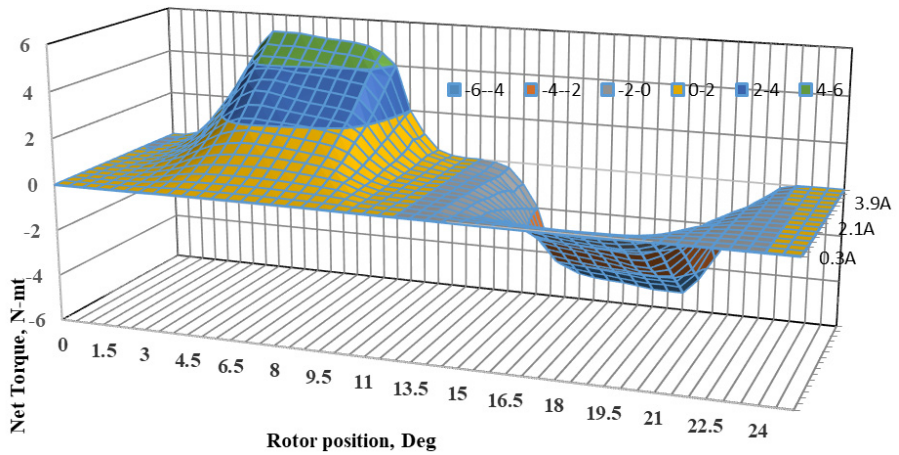


Figure 6: the resultant torque of the main windings

both rotor position and phase currents and is having maximum values when the rotor teeth aligned with stator teeth in both directions.

2.3. Rotor modelling (suspension control)

The total suspension force (F_s) is obtained with the adding of both X and Y-directional suspension forces to levitate the rotor from a standstill position, according to equations (1), (2).

$$F_s = F_x + F_y \quad (1)$$

$$F_s = m \left[\frac{d^2x}{dt^2} + \frac{d^2y}{dt^2} \right] + [k_x + k_y] + m_g. \quad (2)$$

The desired rotor displacement tracking states are given by equation (3) by choosing the displacement states X1, X2, Y1, Y2 as state variables from (1), (2).

$$\begin{aligned} \dot{x}_1 &= x_2, & \dot{Y}_1 &= Y_2, \\ \dot{X}_2 &= -\frac{k_x}{m}X_1 + \frac{F_x}{m} + F_{dx}, & \dot{Y}_2 &= -\frac{k_y}{m}Y + \frac{F_y}{m} + F_{dy} + g. \end{aligned} \quad (3)$$

The electrical equivalent suspension forces in terms of suspension currents are given by equation (4).

$$\begin{bmatrix} F_x \\ F_y \end{bmatrix} = \begin{bmatrix} K_{x xp} & K_{x yp} & K_{x xn} & K_{x yn} \\ K_{y xp} & K_{y yp} & K_{y xn} & K_{y yn} \end{bmatrix} \begin{bmatrix} i_{xp}^2 \\ i_{yp}^2 \\ i_{xn}^2 \\ i_{yn}^2 \end{bmatrix}. \quad (4)$$

Equations (5) and (6) can be obtained from equations (3) and (4),

$$F_x = m \frac{d^2x}{dt^2} + k_x = [K_X][I_x], \quad (5)$$

$$F_y = m \frac{d^2y}{dt^2} + k_y + mg = [K_Y][I_Y], \quad (6)$$

where, $K_X = \text{diag} \left[K_{x xp} \ K_{x yp} \ K_{x xn} \ K_{x yn} \right]$,
 $K_Y = \text{diag} \left[K_{y xp} \ K_{y yp} \ K_{y xn} \ K_{y yn} \right]$ and

$$I_x = \begin{bmatrix} I_{xp}^2 \\ I_{xn}^2 \end{bmatrix}, \quad I_Y = \begin{bmatrix} I_{yp}^2 \\ I_{yn}^2 \end{bmatrix}.$$

For the rotor displacements, the equivalent desired tracking state-space equations are given by equation (7).

$$\begin{bmatrix} \dot{x}_1 \\ \dot{x}_2 \\ \dot{y}_1 \\ \dot{y}_2 \end{bmatrix} \begin{bmatrix} 1 & 0 & 0 & 0 \\ -\frac{k}{m} & 0 & 0 & 0 \\ 0 & 0 & 1 & 0 \\ 0 & 0 & -\frac{k}{m} - g & 0 \end{bmatrix} \begin{bmatrix} x_1 \\ x_2 \\ y_1 \\ y_2 \end{bmatrix} + \begin{bmatrix} 0 & 0 & 0 & 0 \\ K_{xyp} & K_{xyp} & K_{xxn} & K_{xyn} \\ 0 & 0 & 0 & 0 \\ K_{yxp} & K_{yyp} & K_{yxn} & K_{yyn} \end{bmatrix} \times \begin{bmatrix} i_{xp}^2 \\ i_{yp}^2 \\ i_{xn}^2 \\ i_{yn}^2 \end{bmatrix}. \quad (7)$$

2.4. Modelling of BSRM for torque control

The motor states Ψ_{ph} , w and θ are considered as state variables for the state-space representation of BSRM according to Eq. (8).

$$\begin{aligned} \frac{d\psi_{ph}}{dt} &= -R_{ph}N(\theta)\psi_{ph} + V_{ph} + w_{\psi}, & \frac{dw}{dt} &= \frac{T_e - T_l}{J} - \frac{B}{J}w + \frac{T_e}{J} + w_w, \\ \frac{d\theta}{dt} &= w + w_{\theta}, \\ I_{ph} &= N(\theta)\psi_{ph}. \end{aligned} \quad (8)$$

2.5. Switching control strategy

The BSRM needs an overall six hysteresis current controllers for controlling both suspension force and net torque. Out of six, two are for individual torque winding current controllers, and the remaining four are for suspension force current controllers. According to the operating principle, the six-phase 12/14 BSRM needs 12 power switches. As a result, eight power switches are essential for controlling the four-phase suspension windings and four power switches for two-phase torque windings.

Figure 7 shows the four switching states of the asymmetric converter, which are used in BSRM for independent control of each phase: mode 1 is a magnetization mode in which positive DC-link voltage has applied to the winding; Mode 2 and 3 are freewheeling modes in which the winding has short-circuited through an IGBT and a diode; Mode 4 is demagnetization mode where the negative DC-link voltage has applied.

The selection of suspending force windings are shown in Table 2: the switching state 1 indicates magnetization mode, where the switching state 0 means freewheeling mode.

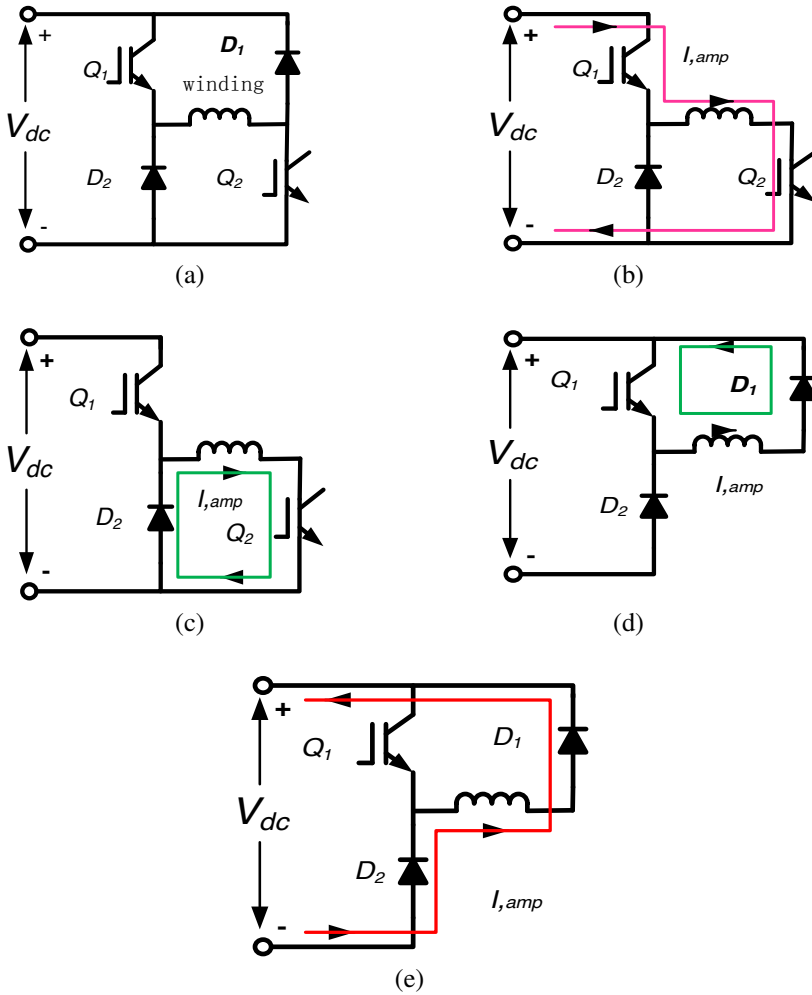


Figure 7: Asymmetric Converter Switching Modes: (a) Ideal Mode, (b) mode 1 (Q_1 : On, Q_2 : On), (c) mode 2 (Q_1 : Off, Q_2 : On), (d) mode 3 (Q_1 : On, Q_2 : Off), (e) mode 4 (Q_1 : Off, Q_2 : Off)

Table 2: Hysteresis current control switching states for BSRM

Desired force	Suspending force poles selection	I_{s1}	I_{s2}	I_{s3}	I_{s4}
If $F_x \geq 0, F_y \geq 0$	I_{s1} and I_{s2}	1	1	0	0
If $F_x \geq 0, F_y \leq 0$	I_{s2} and I_{s3}	0	1	1	0
If $F_x \leq 0, F_y \leq 0$	I_{s3} and I_{s4}	0	0	1	1
If $F_x \leq 0, F_y \geq 0$	I_{s4} and I_{s1}	1	0	0	1

3. Proposed square currents control method with sliding mode torque observer

In the conventional method, the reference current, $I_{ref} = I_a + I_b$, is controlled by two current sensors and transducers. The torque ripple occurs during phase commutation when only the addition of the phase currents have controlled because of the uncontrolled phase currents at the increasing period (in real cases, the torque varies with the square of the phase currents). Thus, the sum of the square currents, $I_{ref}^2 = I_a^2 + I_b^2$, should be controlled. The simple block diagram of a square currents control block diagram is shown in Fig. 8. The proposed control algorithm needs at least two current sensors along with analogue multipliers. A sensorless sliding mode torque observer has modelled to avoid sensors and makes the system simple and economical.

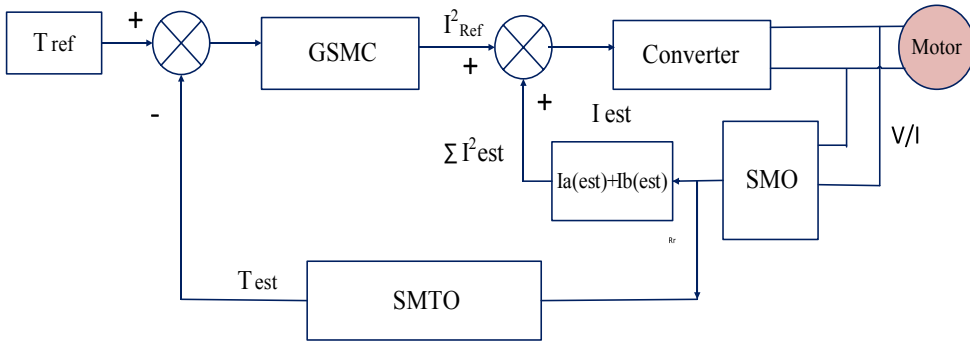


Figure 8: Simple square currents control block diagram

GSMC can implement a closed-loop direct torque control using the instantaneous torque estimation. GSMC contains a torque hysteresis-controller, which used for generating the switching signals for all activated motor phase windings. Table 2 lists the switching signal states and its functions. The extra exponential fast decaying nonlinear term and tracking error torque functions are considered in the global sliding mode switching surface to get fast response and less chattering.

The torque tracking error function is defined by Eq. (9)

$$e_T = T_{est} - T_{ref} \quad (9)$$

The torque tracking switching function is given by Eq. (10)

$$S_T = \dot{e}_T + C_T e_T - S_T(0)e^{-kt}, \quad C_T > 0. \quad (10)$$

By using new switching functions (10), the proposed global sliding mode torque controller equation is derived and shown in (11). The resulting dynamic

closed-loop torque controller guarantees the desired torque when $t \rightarrow \infty$.

$$U_T = -J_{\text{new}} (C_w w - \dot{f}(t)) + J_{\text{new}} (\dot{T}_{\text{ref}} + C_T T_{\text{ref}}) \\ [4pt] - (\Delta J_{\text{new}} |C_T T_{\text{act}} - \dot{f}(t)| + \Delta J |\dot{T}_{\text{ref}} + C_T T_{\text{ref}}|) \text{sgn}(s_T). \quad (11)$$

Global sliding mode torque control simple block diagram of BSRM is shown in Fig. 9.

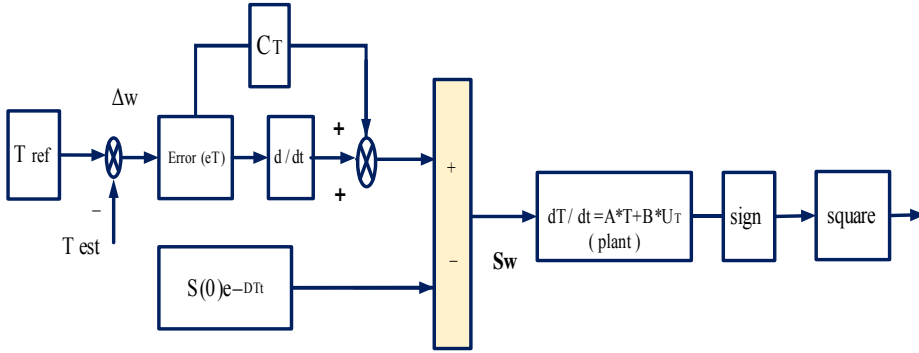


Figure 9: Torque control block diagram of GSMC

From the individual phase currents and voltages, the sliding mode observer dynamics are given by Eqs. (12)–(14).

$$\frac{d\hat{w}}{dt} = \frac{\hat{T}e}{J} - \frac{B}{J}\hat{w} + K_w \text{sign}(\hat{i} - i), \\ \frac{d\hat{\theta}}{dt} = \hat{w} + K_\theta \text{sign}(\hat{i} - i), \quad (12) \\ \hat{T}_{est} = \hat{T}_e(i, \hat{\theta}),$$

$$S = \hat{i} - i = \begin{bmatrix} N_0 & 0 & M_0 \end{bmatrix} \begin{bmatrix} \hat{\psi} - \psi & \hat{w} - w & \hat{\theta} - \theta \end{bmatrix}^T, \quad (13)$$

$$S = N_0 e_\psi + M_0 e_\theta, \quad \dot{S} = N_0 \dot{e}_\psi + M_0 \dot{e}_\theta, \quad (14)$$

where the symbol $\hat{\cdot}$ denotes the corresponding observed. The switching gain constants K_ψ , K_w and K_θ are needs a careful design for the SMO successful operation because the whole observer output states are consists the corresponding terms of the product of pre-determined switching gain constants to the corresponding error functions. The proposed torque control block diagram is shown in Fig. 9, along with error terms of current and positions. The equivalent structure of the sliding mode observer is shown in Fig. 10.

The detailed overall control scheme and observer technics are shown in Fig. 11.

4. Results and discussions

A set of experiments have been carried out to get the smooth torque control and rated speed. The phase voltage and current quantities are sampled simultaneously at one instant and sent to SMTO. The total machine torque has been obtained by adding the individually estimated phase torques of both phases. This net estimated torque has been analyzed together with the reference torque. The torque error tracking based GSMC makes the drive robust against any sudden loads. The SMTO measures the rotor position after 100 micro-secs when the rotor is at any preliminary rotor position.

Figures 12a and b show that the proposed torque observer could quickly measure the suspension parameters in less than 0.0001 sec.

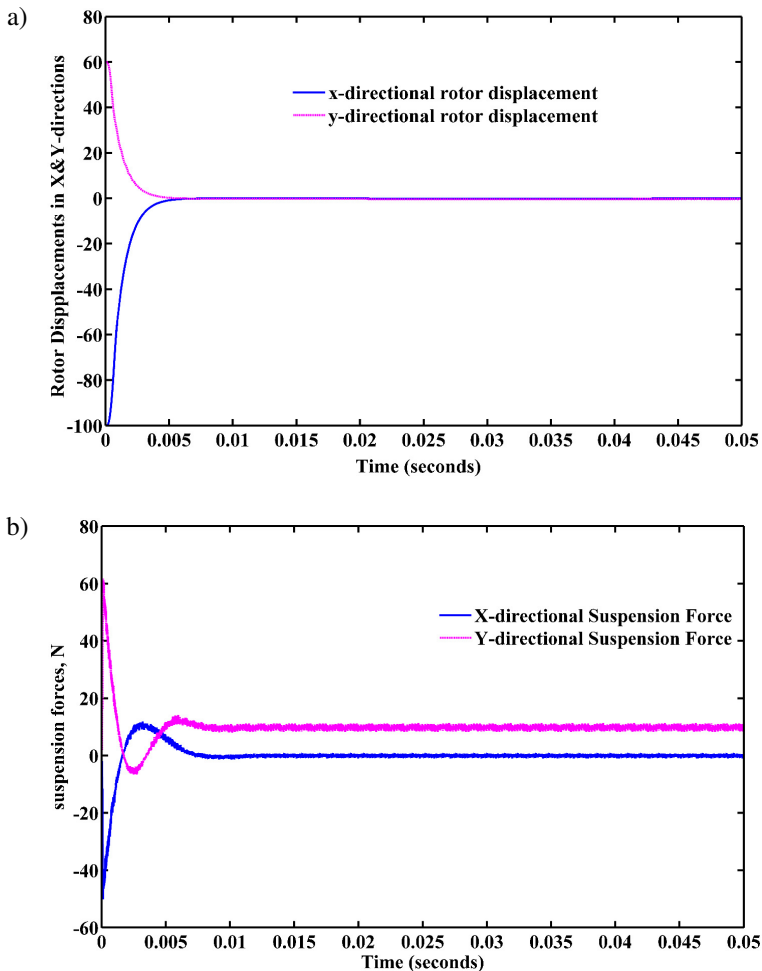


Figure 12: (a) X-Y rotor Displacements; (b) X-Y rotor suspension forces

Similarly, the SMTO measures the motor parameters quickly (see Fig. 13). Figure 13a–e) show the regulated phase Voltages, actual and estimated phase currents and phase–A and phase–B rotor positions, respectively. From the actual and estimated phase currents, Figure 13b and c, it is observed that the error current between the actual and measured currents of both the phases are very nearly less than 0.05 A, which indicates that the observer currents are practically the same as the actual currents.

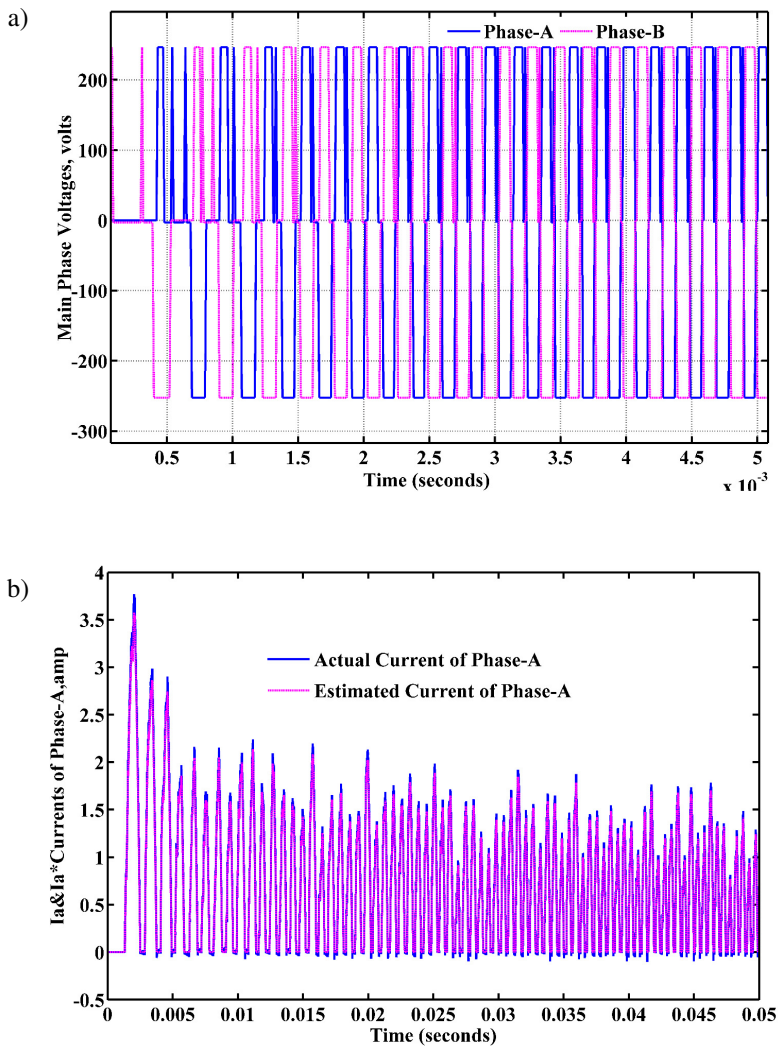


Fig. 13 a, b

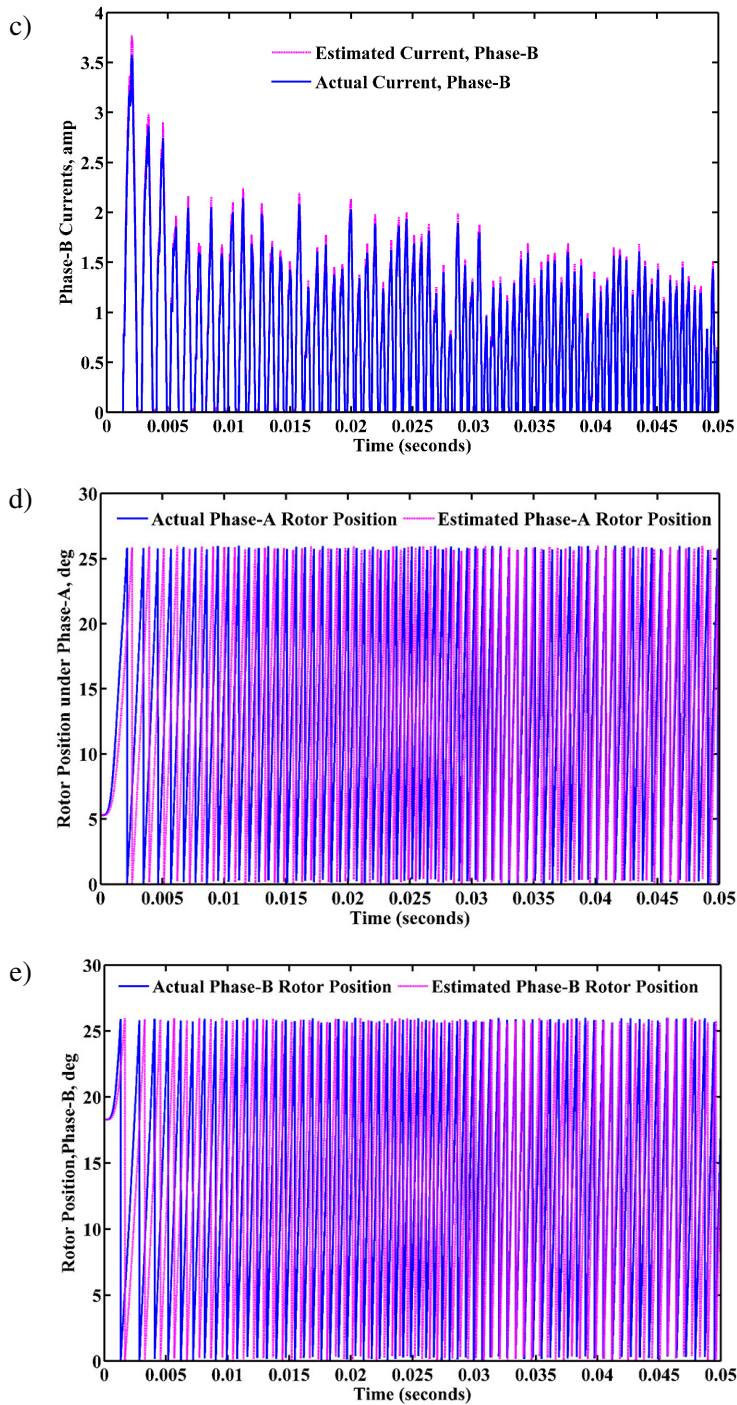


Figure 13: (a) The single pulse controlled main Phase Voltages; (b) Phase-A actual and measured currents; (c) Phase-B actual and measured currents; (d) Phase-A actual and estimated rotor positions; (e) Phase-B actual and estimated rotor positions

4.1. Measurements in normal condition

Figures 14a to b show the rated speed, actual and estimated torques without proposed method respectively. It is detected in Fig. 14b that the actual torque contains both positive and negative ripples because there is no method is used to reduction of torque ripple in the actual system, but the torque observer's torque contains simply positive ripples and no more negative ripples because of sensor-less observer operation.

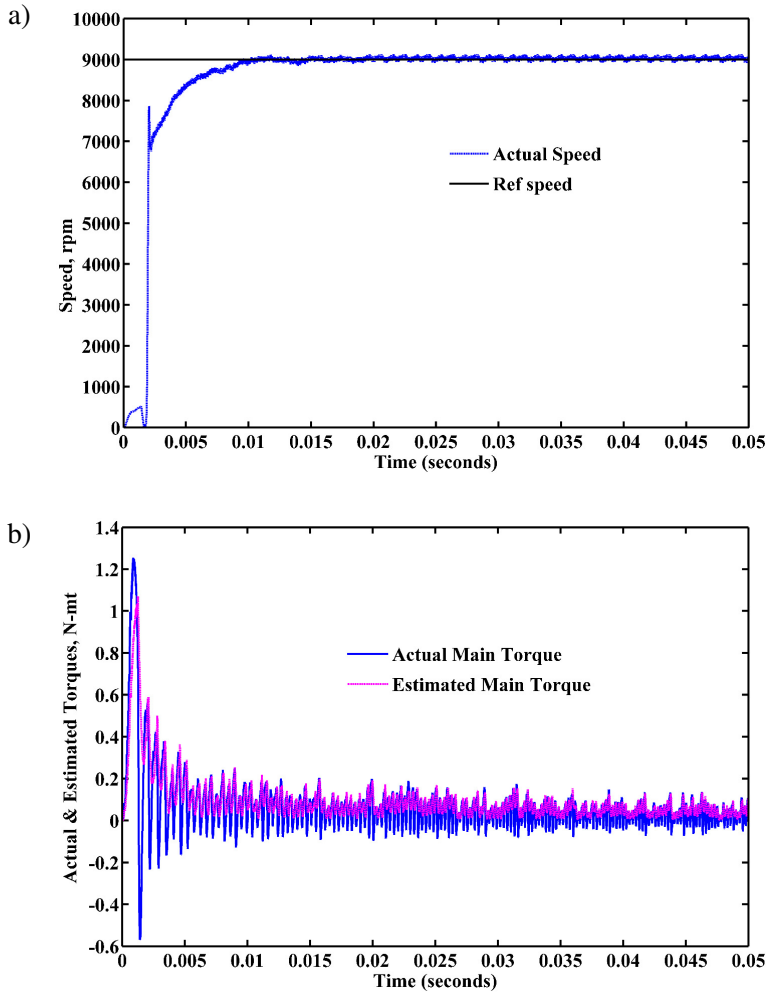


Figure 14: (a) Rated speed; (b) Actual and estimated Torques without Square Currents control

Figure 15 shows the actual and estimated torques with the proposed control method at normal conditions. Figure 15 shows that the torque ripples are mostly

minimized both in actual and estimated torques, likewise, the actual torque profile maintains the high average torque value by using proposed square currents control with GSMC.

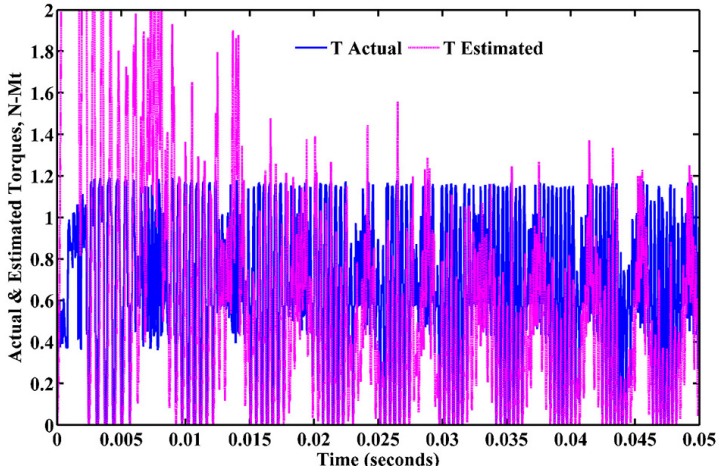


Figure 15: Actual and estimated torques with square currents control method at normal condition

4.1.1. Torque loads are changed

The value of 0.8 N-mt torque load is added suddenly at 0.02 sec, and the same load is removed at 0.04 sec, showing the quick and robust tracking properties of SMTO. Figure 16 shows that the torque observer can rapidly track the torque

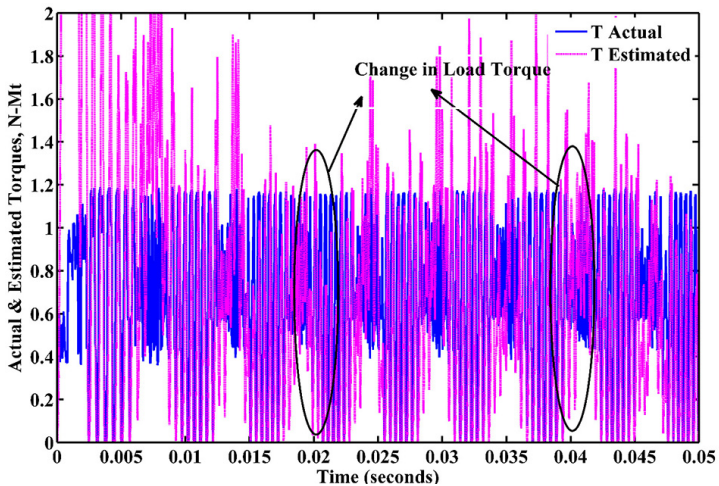


Figure 16: Actual and measured torques when external torque loads applied

in less than 0.001 sec. The proposed method shows the improvement in torque profile according to Fig. 16, and there were no negative torques. Hence, the average torque increased quietly.

4.1.2. Supply voltage changed

The proposed method of behaviour is studied by varying phase voltages. There is a chance of the sudden change in voltages in the converters and excitation system. In this study, the phase voltage is varied from 250 V to 200 V at 0.02 sec, and from 200 V to 250 V at 0.04 sec. The resultant torque profiles are shown in Fig. 17. The input voltage changes suddenly, both actual and measured quantities of torque response do not change rapidly because of the sliding mode control and observer switching surface properties.

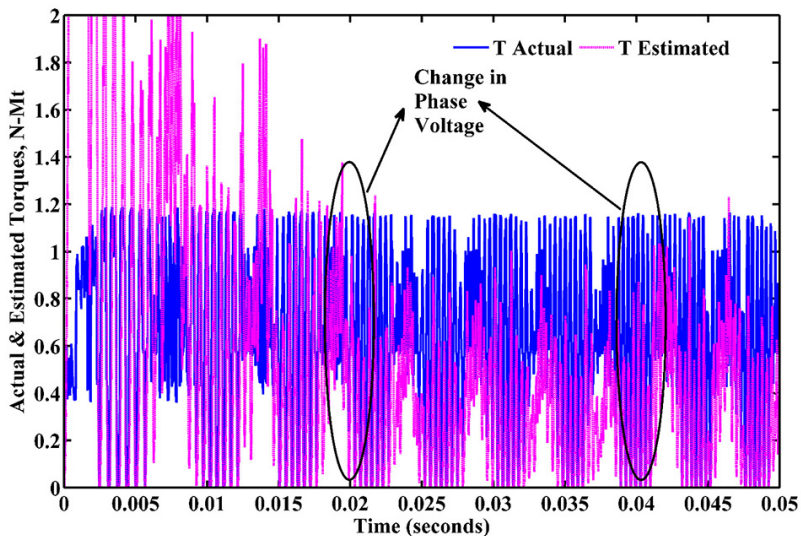


Figure 17: Actual and estimated torques

4.1.3. Switching angle is changed

The acoustic noise rises when then switching turn-off angle is close to the aligned position and the noise reduces when the switching angle as forwarding conduction angle, but the advanced switching angle operation effects decrease the efficiency of the motor. Whenever the torque ripple decreases in the switched reluctance motor, the noise also reduces. Therefore, it could be indicated that the variation and selection of the switching angles are a significant reason for torque ripple reduction. The measured and actual torque profiles are presented in Figs. 18a and b when the switching angles are varied from 12 deg to 13 and 11 deg respectively at 0.02 sec. Figures 18a and b show both measured and actual

torques are less varied, and there are no negative torque ripples, i.e., the average torque profile is increased and maintained robust behaviour even under switching angle variations.

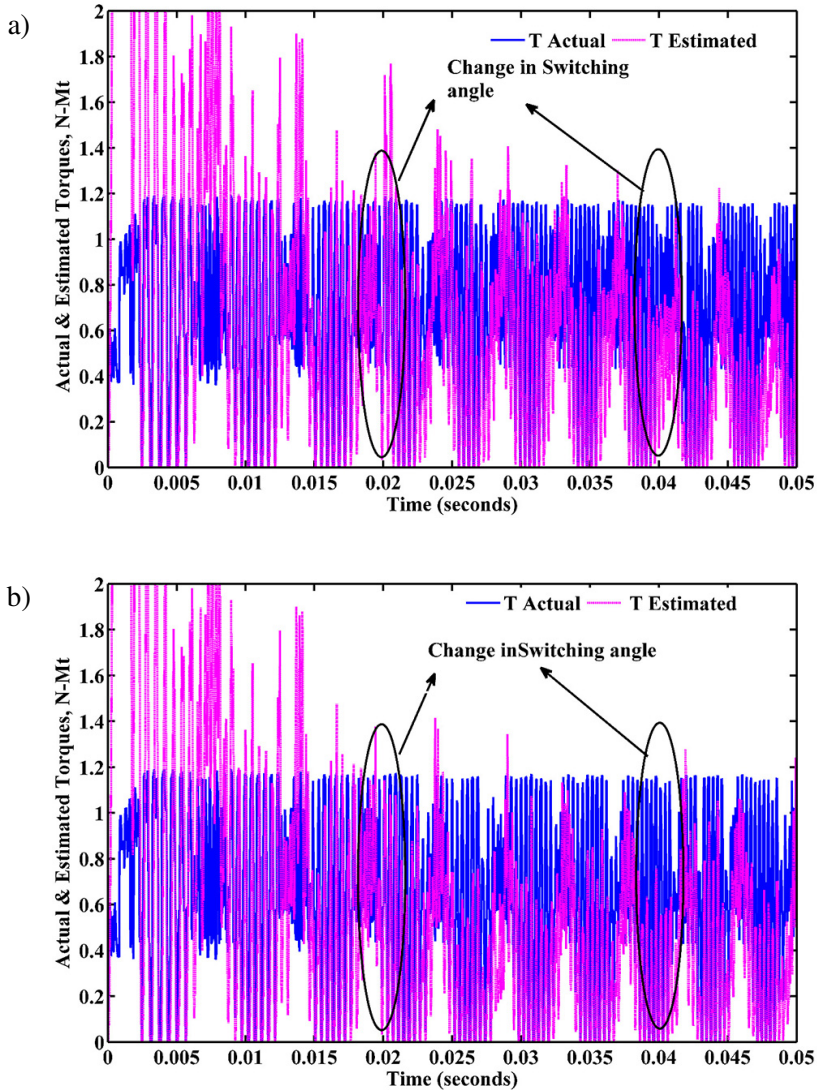


Figure 18: (a) Actual and measured torques when switching angle changed to 13 deg; (b) Actual and measured torques when switching angle changed to 11 deg

All parameters variation conditions the SMTO can exhibit a stable and robust estimation according to the previous results. The proposed controlled square currents method with SMTO not only reduces the torque ripples, but it also

increases the average value of actual torque and controls the overall system stably, even though the electrical and mechanical parameters changed. However, the whole torque ripple reduction is unattainable practically due to the interaction of the different mechanical parts of the BSRM.

4.2. Analysis of torque profiles of the proposed method with the SMC based SMTO

Figures 19a–e present comparison diagrams, the conventional SMC and proposed GSMC based SMTO offers a steady torque measurement when BSRM has subjected to parameter deviations. Both control technics tracks the torque in less than 0.001 sec, and there are no negative torque ripples produced in actual and estimated torques. The actual torque of the proposed method shows the less ripple and high average value than the conventional method.

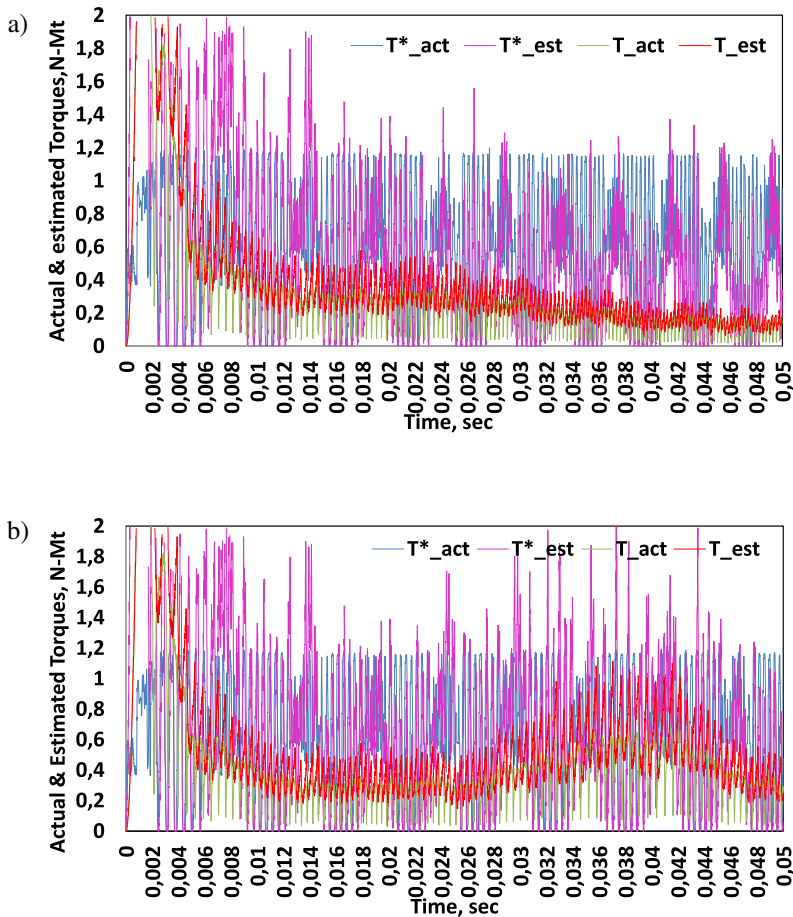


Fig. 19 a, b

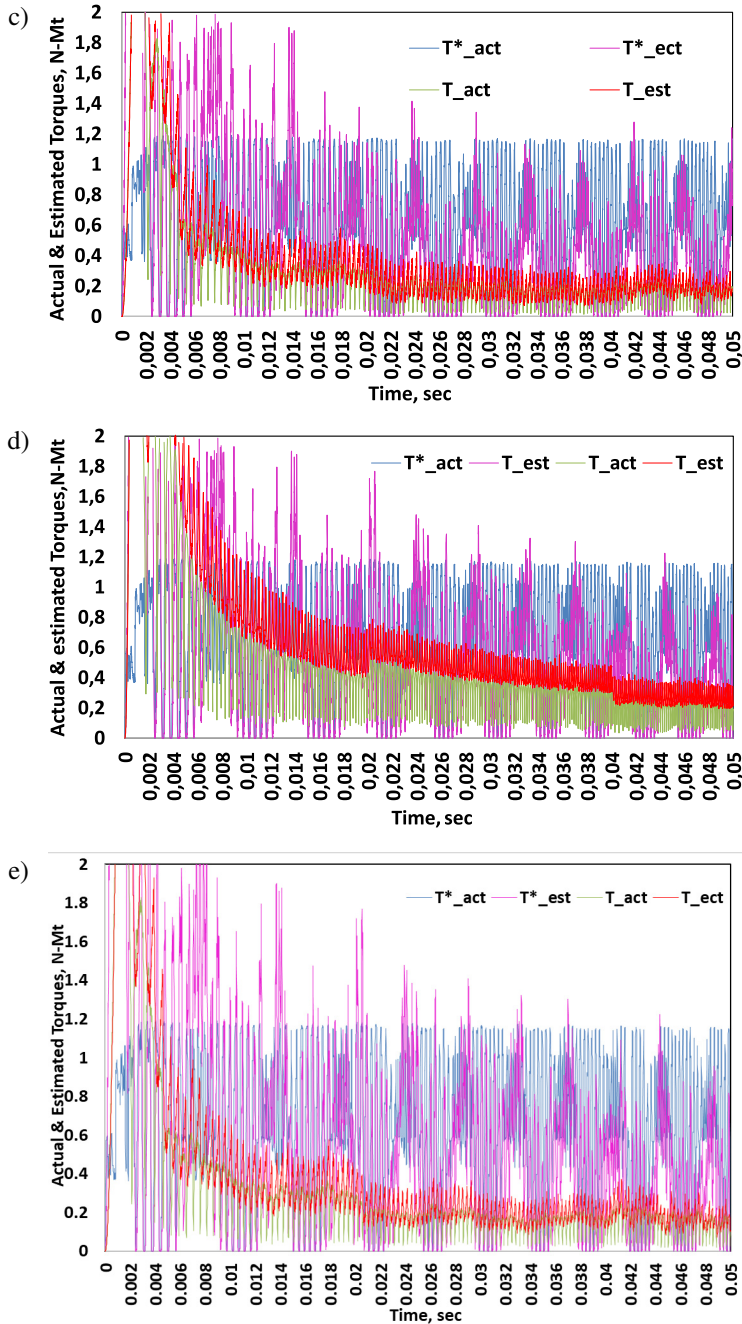


Figure 19: (a) Actual and measured torques healthy condition; (b) actual and measured torques when load torque applied; (c) actual and measured torques when switching angle changed to 11 deg; (d) actual and measured torques when switching angle changed to 13 deg; (e) actual and measured torques when the phase voltage varied

5. Conclusions

The GSMC based SMTO with the proposed square currents control method proves the right choice for the nonlinear systems like BSRM system. To this end, the proposed method shows the following essential advantages in comparison to other torque ripple reduction techniques.

- Instantaneous torque estimation was done solely with terminal voltage, and current.
- Instantaneous torque control has done without using mechanical sensors
- Quick measurement and fast response even in under loading conditions.
- There are no negative torque ripples produced in both actual and estimated torques, and the average torque value increased.
- More stable and high robustness against parametric variations.

Nomenclature

Variable name	Description
m	Rotor mass, kg
g	Gravity, (9.8 m/s ²)
F_x, F_y	X and Y-directional Suspension forces respectively
ψ_{ph}	Flux linkage of torque winding
R_{ph}	Resistance of torque winding, ohms
N_{ph}	Reversal matrix vector of inductance.
θ_{ph}	Per phase rotor position, [deg].
V_{ph}	Torque winding voltage in per phase, [volts].
w	Net speed, [rpm].
T_e and T_l	Motor torque and load torque, [Nt-m]
$B, J, J_{new}, \Delta J$	Damping constant, rotor moment of inertia and $J_{new} = \frac{J_{max} + J_{min}}{2}, \Delta J = \frac{J_{max} - J_{min}}{2}$
i	Phase current vector, A.
e_x, e_y, e_T	Error displacements of the rotor in X and Y directions and error torque vectors, respectively.
C_x, C_y, C_T	Positive switching function constants of rotor displacements and torque, respectively.

D_x, D_y, D_T	Exponential switching constants of Rotor displacements and torque respectively.
S_x, S_y, S_T	Rotor X and Y displacement and torque switching equations, respectively.
U_x, U_y, U_T	Rotor displacement and torque control equations respectively.

References

- [1] M. CHAPLE, S. BODKHE, and P. DAIGAVANE: Torque ripple minimization in switch reluctance motor drives: An ANFACO based control, *International Journal of Intelligent Engineering and Systems*, **11**(4), (2018), 264–274, DOI: [0.22266/ijies2018.0831.26](https://doi.org/10.22266/ijies2018.0831.26).
- [2] S. JEBARANI EVANGELINE and S. SURESH KUMAR: Torque ripple minimization of switched reluctance drives – A survey, *IET Conference Publications*, 2010(563 CP), (2010), 1024–1028, DOI: [10.1049/cp.2010.0177](https://doi.org/10.1049/cp.2010.0177).
- [3] I. HUSAIN and M. EHSANI: Torque ripple minimization in switched reluctance motor drives by PWM current control, *IEEE Transactions on Power Electronics*, **11**(1) (1996), 83–88, DOI: [10.1109/63.484420](https://doi.org/10.1109/63.484420).
- [4] X. ZHANG, Q. YANG, M. MA, Z. LIN, and S. YANG: A switched reluctance motor torque Ripple reduction strategy with deadbeat current control and active thermal management, *IEEE Transactions on Vehicular Technology*, **69**(1), (2020), 317–327, DOI: [10.1109/TVT.2019.2955218](https://doi.org/10.1109/TVT.2019.2955218).
- [5] X. GAO, X. WANG, Z. LI, and Y. ZHOU: A review of torque ripple control strategies of switched reluctance motor, *International Journal of Control and Automation*, **8**(4), (2015), 103–116, DOI: [10.14257/ijca.2015.8.4.13](https://doi.org/10.14257/ijca.2015.8.4.13).
- [6] F.P.G. MARQUEZ: An approach to remote condition monitoring systems management. In *2006 IET International Conference On Railway Condition Monitoring*, (2006), 156–160.
- [7] S. OGWONSKI, D. BISMOR, and Z. OGWONSKI: Control of complex dynamic nonlinear loading process for electromagnetic mill, *Archives of Control Sciences*, **30**(3) (2020), 471–500, DOI: [10.24425/acs.2020.134674](https://doi.org/10.24425/acs.2020.134674).
- [8] H. TORKAMAN and E. AFJEI: Comprehensive detection of eccentricity fault in Switched Reluctance Machines using High Frequency Pulse Injection, *IEEE Transactions on Power Electronics*, **28**(3), (2013), 1382–1390, DOI: [10.1109/TPEL.2012.2205947](https://doi.org/10.1109/TPEL.2012.2205947).

- [9] H. CAI, H. WANG, M. LI, S. SHEN, Y. FENG, and J. ZHENG: Torque ripple reduction for switched reluctance motor with optimized PWM control strategy, *Energies*, **11**(11), (2018), DOI: [10.3390/en11113215](https://doi.org/10.3390/en11113215).
- [10] R.S. WALLACE and D.G. TAYLOR: Torque ripple reduction in three-phase switched reluctance motors, *Proceedings of the American Control Conference*, **22** (1990), 1526–1527, DOI: [10.23919/acc.1990.4790992](https://doi.org/10.23919/acc.1990.4790992).
- [11] N. INANC and V. OZBULUR: Torque ripple minimization of a switched reluctance motor by using continuous sliding mode control technique, *Electric Power Systems Research*, **66**(3), (2003), 241–251, DOI: [10.1016/S0378-7796\(03\)00093-2](https://doi.org/10.1016/S0378-7796(03)00093-2).
- [12] H.S. RO, H.G. JEONG, and K.B. LEE: Torque ripple minimization of switched reluctance motor using direct torque control based on sliding mode control, *IEEE International Symposium on Industrial Electronics*, 2013, DOI: [10.1109/ISIE.2013.6563641](https://doi.org/10.1109/ISIE.2013.6563641).
- [13] F.P.G. MÁRQUEZ: A new method for maintenance management employing principal component analysis, *Structural Durability and Health Monitoring*, **6**(2), (2010), 89–100, DOI: [10.3970/sdhm.2010.006.089](https://doi.org/10.3970/sdhm.2010.006.089).
- [14] H.A. MAKSOUD: Torque ripple minimization of a switched reluctance motor using a torque sharing function based on the overlap control technique, *Engineering, Technology and Applied Science Research*, **10**(2), (2020), 5371–5376,
- [15] N. SAHA, A.K. PANDA and S. PANDA: Speed control with torque ripple reduction of switched reluctance motor by many optimizing liaison technique, *Journal of Electrical Systems and Information Technology*, **5**(3), (2018), 829–842, DOI: [10.1016/j.jesit.2016.12.013](https://doi.org/10.1016/j.jesit.2016.12.013).
- [16] M.M. BOUIABADY, A.D. ALIABAD and E. AMIRI: Switched reluctance motor topologies: A comprehensive review. In *Switched Reluctance Motor – Concept, Control and Applications*, A. Tahour and A.G. Aissaoui (Eds.), 1–24, 2017, DOI: [10.5772/intechopen.69149](https://doi.org/10.5772/intechopen.69149).
- [17] P. MORENO-TORRES, M. LAFOZ, M. BLANCO, G. NAVARRO, J. TORRES and L. GARCÍA-TABARÉS: Switched reluctance drives with degraded mode for electric vehicles. In *Modeling and Simulation for Electric Vehicle Applications*, M.A. Fakhfakh (Ed.), 2016, DOI: [10.5772/64431](https://doi.org/10.5772/64431).
- [18] X. ZAN: Switched reluctance motor speed performance simulation study based on torque ripple suppression, *International Conference on Advanced Mechatronic Systems, ICAMechS*, **1** (2013), 253–257, DOI: [10.1109/ICAMechS.2013.6681789](https://doi.org/10.1109/ICAMechS.2013.6681789).

- [19] M. ZHU, Y. ZHANG, Z. XIE, and B. ZHAO: Method of reducing noise and torque ripple of switched reluctance motor, *Proceedings – 2017 Chinese Automation Congress, CAC 2017*, **2017**(1), 2761–2765, DOI: [10.1109/CAC.2017.8243245](https://doi.org/10.1109/CAC.2017.8243245).
- [20] M.A. HAMIDA, Z. TIR, E. OUED, O.P. MALIK, F. MARIGNETTI and C. FROSI-NONE: Sensorless control of switched reluctance machine based on nonlinear observer and fuzzy logic controller. In *4th International Conference on Recent Advances in Electrical Systems*, Tunisia, (2019), paper 89.
- [21] T. YUVAPRIYA, P. LAKSHMI, and S. RAJENDIRAN: Vibration control and performance analysis of full car active suspension system using fractional order terminal sliding mode controller, *Archives of Control Sciences*, **30**(2), (2020), 295–324, DOI: [10.24425/ACS.2020.133501](https://doi.org/10.24425/ACS.2020.133501).
- [22] W. SHANG, S. ZHAO, Y. SHEN, and Z. QI: A sliding mode flux-linkage controller with integral compensation for switched reluctance motor, *IEEE Transactions on Magnetics*, **45**(9), (2009), 3322–3328, DOI: [10.1109/TMAG.2009.2021264](https://doi.org/10.1109/TMAG.2009.2021264).
- [23] M.M. KHATER: A sliding mode observer-based sensorless switched reluctance motor drive, *Engineering Research Journal*, Faculty of Engineering, Minoufiya University, Egypt, **29**(4), (2006), 329–335.
- [24] Z. HAO, Q. YU, X. CAO, X. DENG and X. SHEN: An improved direct torque control for a single-winding bearingless switched reluctance motor, *IEEE Transactions on Energy Conversion*, **35**(3), (2020), 1381–1393, DOI: [10.1109/tec.2020.2988549](https://doi.org/10.1109/tec.2020.2988549).
- [25] L. SENTHIL MURUGAN and P. MARUTHUPANDI: Sensorless speed control of 6/4-pole switched reluctance motor with ANFIS and fuzzy-PID-based hybrid observer. *Electrical Engineering*, 102 (2020), 831-844, DOI: [10.1007/s00202-019-00915-5](https://doi.org/10.1007/s00202-019-00915-5).
- [26] K. YOVCHEV, K. DELCHEV, and E. KRASDEV: Constrained output iterative learning control, *Archives of Control Sciences*, **30**(1), (2020), 157–176, DOI: [10.24425/ACS.2020.132590](https://doi.org/10.24425/ACS.2020.132590).
- [27] B.H. CHOI, Y. PARK, Y. CHO, and M. LEE: Global sliding-mode control. Improved design for a brushless DC motor, *IEEE Control Systems Magazine*, **21**(3), (2001), 27–35, DOI: [10.1109/37.924795](https://doi.org/10.1109/37.924795).
- [28] Z. CHENG, C. HOU, and X. WU: Global sliding mode control for brushless DC motors by neural networks, *2009 International Conference on Artificial Intelligence and Computational Intelligence, AICI 2009*, **4**(2), (2009), 3–6, DOI: [10.1109/AICI.2009.366](https://doi.org/10.1109/AICI.2009.366).

- [29] S.K. SPURGEON: Sliding mode observers: A survey, *International Journal of Systems Science*, **39**(8), (2008), 751–764, DOI: [10.1080/00207720701847638](https://doi.org/10.1080/00207720701847638).
- [30] R.A. McCANN and M.S. ISLAM: Application of a sliding-mode observer for position and speed estimation in switched reluctance motor drives, *IEEE Transactions on Industry Applications*, **37**(1), (2001), 51–58, DOI: [/10.1109/28.903126](https://doi.org/10.1109/28.903126).
- [31] Y.J. ZHAN: A novel sliding-mode observer for indirect position sensing of switched reluctance motor drives. *IEEE Transactions on Industrial Electronics*, **46**(2), (1999), 390–397, DOI: [10.1109/41.753778](https://doi.org/10.1109/41.753778).
- [32] M.S. ISLAM, I. HUSAIN, R.J. VEILLETTE, and C. BATUR: Design and performance analysis of sliding-mode observers for sensorless operation of switched reluctance motors, *IEEE Transactions on Control Systems Technology*, **11**(3), (2003), 383–389, DOI: [10.1109/TCST.2003.810375](https://doi.org/10.1109/TCST.2003.810375).
- [33] P. NAGESWARA RAO, G.V. SIVA KRISHNA RAO, and G.V. NAGESH KUMAR: A novel technique for controlling speed and position of bearingless switched reluctance motor employing sensorless sliding mode observer, *Arabian Journal for Science and Engineering*, **43**(8), (2018), 4327–4346, DOI: [10.1007/s13369-017-3027-8](https://doi.org/10.1007/s13369-017-3027-8).
- [34] P.N. RAO, N.M. KUMAR, S. PADMANABAN, M.S.P. SUBATHRA, and A.A. CHAND: A novel sensorless approach for speed and displacement control of bearingless switched reluctance motor, *Applied Sciences (Switzerland)*, **10**(12), (2020), 1–26, DOI: [10.3390/APP10124070](https://doi.org/10.3390/APP10124070).
- [35] M. TAKEMOTO, H. SUZUKI, A. CHIBA, S. MEMBER, T. FUKAO and M.A. RAHMAN: Improved analysis of a bearingless switched, *IEEE Transactions on Industry Applications*, **37**(1), (2001), 26–34, DOI: [10.1109/28.903123](https://doi.org/10.1109/28.903123).
- [36] M. TAKEMOTO, A. CHIBA, and T. FUKAO: A method of determining the advanced angle of square-wave currents in a bearingless switched reluctance motor, *IEEE Transactions on Industry Applications*, **37**(6), (2001), 1702–1709, DOI: [10.1109/28.968181](https://doi.org/10.1109/28.968181).
- [37] M. TAKEMOTO, A. CHIBA, H. AKAGI, and T. FUKAO: Radial force and torque of a bearingless switched reluctance motor operating in a region of magnetic saturation, *IEEE Transactions on Industry Applications*, **40**(1), (2004), 103–112, DOI: [10.1109/TIA.2003.821816](https://doi.org/10.1109/TIA.2003.821816).
- [38] H. WANG, Y. WANG, X. LIU, and J.W. AHN: Design of novel bearingless switched reluctance motor, *IET Electric Power Applications*, **6**(2), (2012), 73–81, DOI: [10.1049/iet-epa.2010.0229](https://doi.org/10.1049/iet-epa.2010.0229).

- [39] D.-H. LEE and J.-W. AHN: Design and analysis of hybrid stator bearingless SRM, *Journal of Electrical Engineering and Technology*, **6**(1), (2011), 94–103, DOI: [10.5370/jeeet.2011.6.1.094](https://doi.org/10.5370/jeeet.2011.6.1.094).
- [40] P.N. RAO, R. DEVARAPALLI, F.P. GARCÍA MÁRQUEZ, and H. MALIK: Global sliding-mode suspension control of bearingless switched reluctance motor under eccentric faults to increase reliability of motor, *Energies*, **13**(20), (2020), DOI: [10.3390/en13205485](https://doi.org/10.3390/en13205485).
- [41] M. FALAHI, F.R. SALMASI, and C. LUCAS: Modified passivity-based control of switched-reluctance motor with speed and load torque observers, *IECON Proceedings (Industrial Electronics Conference)*, **5** (2006), 1077–1081, DOI: [10.1109/IECON.2006.348019](https://doi.org/10.1109/IECON.2006.348019).
- [42] A. CHAIBET, M. BOUKHNIFER, N. OUDDAH, and E. MONMASSON: Experimental sensorless control of switched reluctance motor for electrical powertrain system, *Energies*, **13**(12), (2020), 3081, DOI: [10.3390/en13123081](https://doi.org/10.3390/en13123081).